

Article

Mapping Forest Vertical Structure in Gong-ju, Korea Using Sentinel-2 Satellite Images and Artificial Neural Networks

Yong-Suk Lee ¹, Sunmin Lee ^{1,2,*}  and Hyung-Sup Jung ^{1,3,*} 

¹ Department of Geoinformatics, University of Seoul, 163 Seoulsiripdaero, Dongdaemun-gu, Seoul 02504, Korea; zik@naver.com

² Center for Environmental Assessment Monitoring, Environmental Assessment Group, Korea Environment Institute (KEI), 370 Sicheong-daero, Sejong-si 30147, Korea

³ Department of Geographical Sciences, The University of Maryland, College Park, MD 20742, USA

* Correspondence: smilee@kei.re.kr (S.L.); hsjung@uos.ac.kr (H.-S.J.); Tel.: +82-2-6490-2892 (H.-S.J.)

Received: 29 December 2019; Accepted: 13 February 2020; Published: 1 March 2020



Abstract: As global warming accelerates in recent years, the frequency of droughts has increased and water management at the national level has become very important. In particular, accurate understanding and management of the forest is essential as the water storage capacity of forest is determined by forest structure. Typically, data on forest vertical structure have been constructed from field surveys that are both costly and time-consuming. In addition, machine learning techniques could be applied to analyze, classify, and predict the uncertainties of internal structures in forest. Therefore, this study aims to map the forest vertical structure for estimating forest water storage capacity from multi-seasonal optical satellite image and topographic data using artificial neural network (ANN) in Gongju-si, South Korea. For this purpose, the 14 input neurons of normalized difference vegetation index (NDVI), two types of normalized difference water index (NDWI), two types of Normalized Difference Red Edge Index (NDre), principal component analysis (PCA) texture, and canopy height average and standard deviation maps were generated from Sentinel-2 optical images obtained in spring and fall season and topographic height maps such as digital terrain models (DTM) and digital surface models (DSM). The training/validation and test datasets for the ANN model were derived from forest vertical structures based on field surveys. Finally, the forest vertical classification map, the result of ANN application, was evaluated by creating an error matrix compared with the field survey results. The result showed an overall test accuracy of ~65.7% based on the number of pixels. The result shows that forest vertical structure in Gong-ju, Korea can be efficiently classified by using multi-seasonal Sentinel-2 satellite images and the ANN approach.

Keywords: forest vertical structure; Sentinel-2; WorldDEM; artificial neural network

1. Introduction

Recently, as the importance of water resource management increases due to the occurrence of drought in an environment such as global warming, interest in forests that play a large role in the global water cycle is increasing. Forests with high water storage capabilities contribute to drought as well as flood control [1]. An accurate understanding of forest water storage capacity in water circulation functions is crucial for preventing water-related disasters and for sustainable water management at the national level [2,3]. However, information on the forest vertical structure for estimating the exact water storage capacity of forests is not quantified in most forest regions because of the complexity and continuous change of the forest. Therefore, forest vertical structure information is essential for understanding the water storage function of forests and for quantifying water storage capacity of forest.

As most water resources originate in forests, forests should be well preserved and managed to protect and maintain the quality of downstream rivers, lakes, and seawater [4]. Forests have thick layers of organic matter and high water penetrating soils that hold a lot of rainwater. By regulating the timing of water supply, forests act as a huge reservoir that mitigates the extreme damage caused by water. The forest vertical structure, which is one of the important factors controlling the amount of water the forest can store, is generally divided into four layers of canopy, understory, shrub, and grass [5]. Forests differ in the degree of water storage by major species, and hardwoods have a higher water storage capacity than conifers [6]. Natural forests with a variety of vertical structures have high vitality and high water storage capacity, whereas artificial coniferous forests have low water storage capacity; artificial forests generally have lower levels than natural forests so that forest management can reduce the amount of evapotranspiration and increase the available water resources [7]. Therefore, it is necessary to manage forests with high water storage capacity, considering the vertical structure along with forest species.

In recent years, the Korean Forest Service is investigating forests based on aerial photographs to produce forest maps. It is difficult to figure out the internal structure of the forest with this method, so the vertical structure information is inevitably constructed through field survey by manpower. Due to the characteristic of forest areas that are inaccessible to people, a large amount of budget is required for field surveys in which 70% of the country is mountainous in South Korea. In addition, it takes a certain time to survey a specific region, making it difficult to build data at the same time for multiple regions with delayed updates. Satellite images enable periodic forest mapping as an effective approach to continuous exploration over large areas where human access is not easy or impossible [8–10]. It is not possible to directly estimate the water storage capacity of the forest, but it is possible to estimate the forest vertical structure [11].

For the vegetation researches, an index map using multiple wavelength bands of an image is generally used to detect vegetation characteristics [12]. Indicators widely used in the vegetation field include normalized difference vegetation index (NDVI) [13], normalized difference water index (NDWI) [14], texture, etc. For Sentinel-2 images, the red edge channels can be provided to produce a normalized difference red edge index (NDre) [15]. As the reflectivity of the red edge wavelength band increases in vegetation, it is effectively known for vegetation discrimination [16]. NDVI and Red Edge Band of Sentinel-2 images were used to distinguish field crops and showed its usefulness for classifying vegetation [17]. On the other hand, rather than using many bands for plant or species classification, a method of selecting specific bands suitable for classification and classifying them into several bands by using such as principal component analysis (PCA) [12].

In addition, forest density classifications were conducted by using aerial images and forest textures [18]. The texture information of the forest can be extracted by considering the difference in canopy arrangement between the single-layer structure and the multi-layer structure. The arrangement of crowns is considered uniform in single-layer forests and uneven in multi-layer forests [18]. In this study, Sentinel-2 optic satellite images were used to obtain optical information based on differences in reflectance caused by forests, height, and arrangement of canopy.

As the height of trees is closely related to the vertical structure of forests, Light Detection And Ranging (LiDAR) data are mainly used to measure tree height [19–21]. The height of trees was estimated using digital surface model (DSM) and digital elevation model (DEM) extracted from LiDAR data, and the texture data was derived from the estimated height [22]. However, LiDAR data is time- and cost-consuming such as field surveys, which could lead to a long update cycle. Among the remote sensing satellite images, the optical image only observes the surface information of the forest, and hence there is a limitation in the internal structure observation. In this regard, digital terrain models (DTM) and DSM data, which are already constructed around the world, could be used to reflect forest height components [23]. Research has been conducted to estimate and validate the vertical distribution of forests from DEM data [24,25].

Additionally, machine learning has recently been increasingly utilized in terms of the abundance of data available for learning, including satellite images. Machine learning techniques can be applied based on large amounts of remote sensing data [26] to produce information about continuous internal structures in forest areas with high uncertainty [27–29]. When conducting forest investigations over large areas of high uncertainty, the application of artificial neural networks (ANN) to satellite remote sensing data could be more effective than time- and cost-consuming aerial photography or human surveying. In addition, support vector machines (SVM) [30,31] and decision tree-based models such as random forests [32] and boosted trees [33,34] are being applied to various fields. In this study, the analysis of forest vertical structure using optical satellite images and machine learning of ANN was conducted.

In this study, the analysis of forest vertical structure to estimate forest water capacity from satellite images by using machine learning method. For this purpose, to extract input layers, index map and texture map were prepared from two seasonal Sentinel-2 optical satellite images after preprocessing. In addition, two types of canopy height maps were produced using the difference between two topographic data of DTM and DSM. The 14 input layers were produced considering the vitality of the canopy, the image texture, and the difference in tree height. Finally, the input layers were applied to ANN algorithms with training/validation and test dataset of forest vertical structure data constructed by field survey; the classification map of forest vertical structure was generated. The accuracy of the result map was evaluated through error matrix. The proposed methods for forest vertical structure could be used for establishing a plan for forest water management by enabling more accurate forest water capacity estimation than previous methods.

2. Study Area and Data

The study area is a part of Gongju-si, South Korea where the Charyeong Mountains are located in the north, Gyeryong Mountain is distributed in the southeast, and major tributaries are joined by the Geum River. The study area covers an area of 864.29 km² and is ~400 m above sea level. The study area is climatically located in the mid-latitudes and belongs to a humid continental climate zone. The Charyeong Mountains block the cold north wind so that it is much warmer than the north, but the area is inland basin and influenced by Geum River, the temperature difference between summer and winter is great. Figure 1 shows the study area on the peninsula with the orthoimage of the Sentinel-2. According to the field survey data, this study area is known to have variously deciduous and coniferous trees as natural and artificial forests.

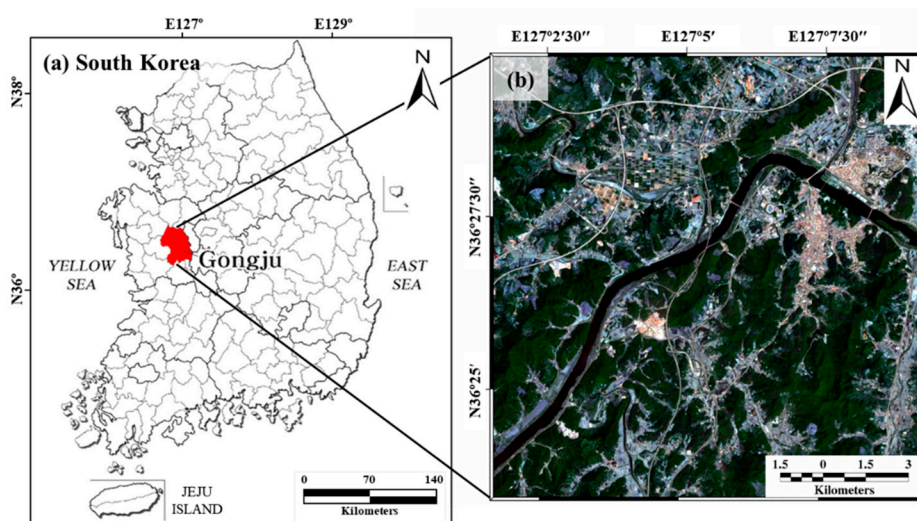


Figure 1. Study area: (a) Gongju, South Korea and (b) Sentinel-2 ortho-rectified image in the study area.

Figure 2 shows (a) three-dimensional structure, (b) major species, (c) artificial and natural forests, and (d) deciduous and coniferous forests from existing vegetation for the vegetation in the study area. Most of the single-layered forests in this area are consists of chestnut artificial forests, whereas the main species of the double-layered forests are natural forests with oyster oak, oak hardwood mixed forests, and pinus rigida artificial forests. In the triple-layered forest, oak natural forest, pinus rigida artificial forest, and oyster-oak tree natural forest are distributed. In this study, the vegetation map of Gongju area was used from the 3rd National Natural Environment Survey conducted by the National Institute of Ecology (NIE) in 2009 [35]. The forest vertical structure data from vegetation map was used as training/validation and test dataset as shown in Figure 2a. In this study, among the canopy layer, the understory layer, and the shrub layer, the layer structure including one or two of layers was defined by the single- and double-layer structure, respectively, whereas the triple-layer structure includes all of the layers.

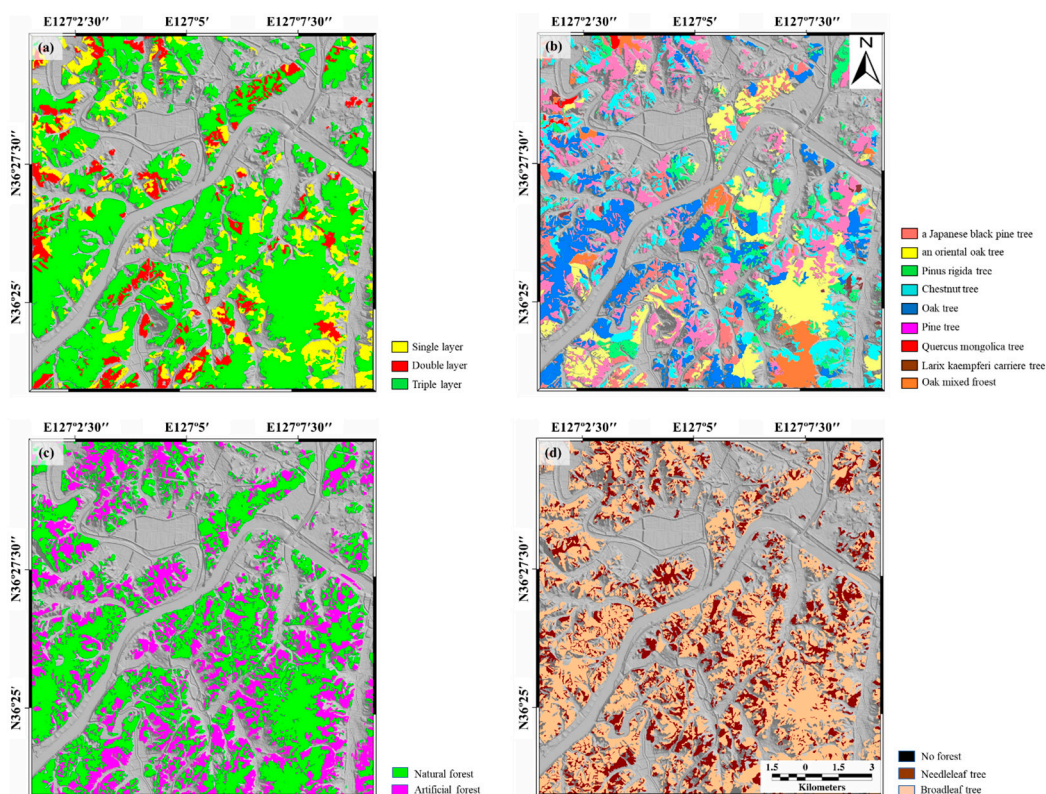


Figure 2. Forest vertical structure classification map of study area constructed by the field survey: (a) Forest vertical structure, (b) dominant species, (c) natural and artificial forests, and (d) dominant species' leaf type [35].

3. Methodology

To map the forest vertical structure, a probability map of forest vertical structure was generated by applying artificial neural network to input layers from (1) Sentinel-2 optical image and (2) DTM (NGII DEM) and DSM (WorldDEM) with the training/validation dataset based on the forest vertical map through fieldwork. Probability maps are classified into single, double, and triple vertical hierarchies, taking into account the characteristics of the forest structures in study area. Finally, test data of field survey data was compared to determine the accuracy of classification through the Error Matrix. Figure 3 shows the overall flow of this study.

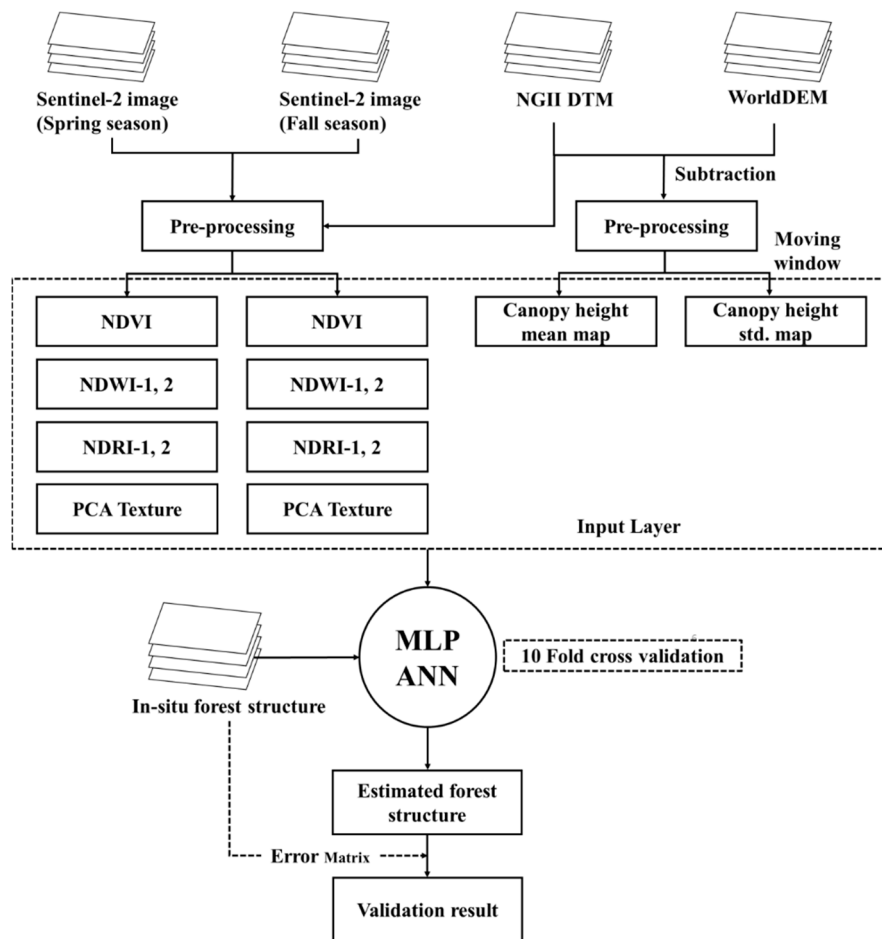


Figure 3. Overall data processing flow to map the forest vertical structure.

3.1. Preprocessing of Input Layers

3.1.1. Preprocessed Layers of Sentinel-2 Images

In this study, two Sentinel-2 images from different seasons of spring and fall were used (European Space Agency (ESA), Paris, France). Figure 4a shows images from 3 May 2017, at 65.3° solar elevation and 143.5° solar azimuth while Figure 4b is from 30 October 2017, with the sun altitude of 38.5° and the azimuth angle of 165.5° (Table 1). The spectral bands defined for the Sentinel-2 used in this study are shown in Table 2. As vegetation, especially hardwoods, could have reflectivity differences depending on the season, images of both seasons were used to account for seasonal characteristics. The NDVI, NDWI, NDre maps, and the PCA texture maps were generated from the Sentinel-2 orthoimages of both seasons by using Matlab (Mathworks, Natick, MA, USA).

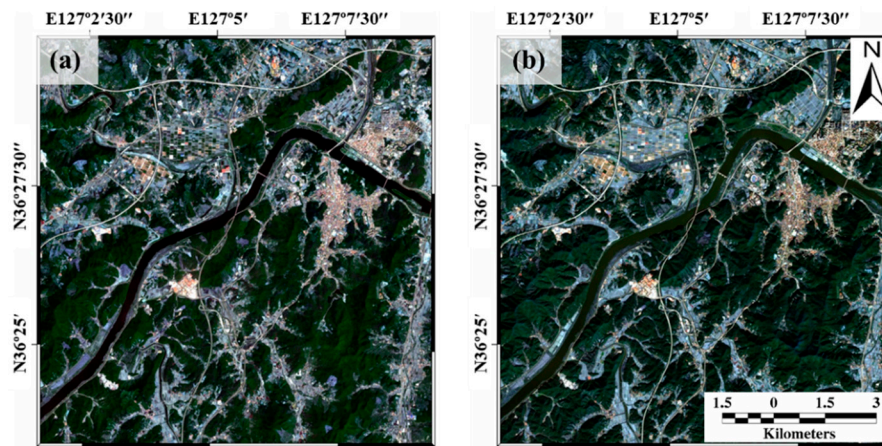


Figure 4. Sentinel-2 satellite ortho-rectified images acquired in the study area: (a) spring season; and (b) fall season.

Table 1. Parameters of Sentinel-2 images used in this study.

Parameters	Spring	Fall
Date (YYYY.MM.DD)	2017.05.03	2017.10.30
Ground sample distance (m)	10	10
Sun altitude angle (deg.)	65.3	38.5
Sun azimuth angle (deg.)	143.5	165.5

Table 2. Definition of Sentinel-2 spectral bands used in this study [36].

Sentinel-2 Bands	Central Wavelength (nm)	Band Width (nm)	Spatial Resolution (m)
3 (Green)	560	35	10
4 (Red)	665	30	10
5 (Vegetation red edge)	705	15	20
6 (Vegetation red edge)	740	15	20
7 (Vegetation red edge)	783	20	20
8 (NIR)	842	115	10
11 (SWIR)	1610	90	20
12 (SWIR)	2190	180	20

Sentinel-2 satellite image data were preprocessed for atmospheric correction and topographic correction. Radiant energy reaches the sensor and is affected by the atmosphere in various ways. Atmospheric correction is a method of eliminating the effects of the atmosphere that disturbs the image by reaching the sensor with unnecessary energy by the atmosphere [36]. Thus, in this study, Sentinel-2 image was converted to Bottom-Of-Atmosphere, which ignores the atmospheric effects of the original image [37]. Atmospheric correction of Sentinel images was performed with a tool called Sen2Cor from Sentinel Application Platform (SNAP) provided by ESA.

In addition, the satellite image data has a difference in reflectivity according to the sun incidence angle in a mountain area with the slope land; high mountainous region has shade and sunlit slopes. Topographic correction is necessary for mountainous area to minimize other impacts besides the forest features. In this study, a commonly used terrain correction model of statistical-empirical correction [38] was applied to Sentinel-2 optical image as follows,

$$\rho_h = \rho - \{a \cdot \cos i + b\} + \bar{\rho} \tag{1}$$

where ρ and ρ_h are pixel values from original and topographic-corrected images, respectively, $\bar{\rho}$ is the mean value of the original image and i indicates the incidence angle. a and b are parameters of the statistical empirical model.

After the topographic correction process, NDVI, NDWI, and NDre maps are generated from the topographic-corrected Sentinel-2 images, which were used for forest vertical mapping in this study instead of the original image. NDVI is an index based the reflectance difference between red and near-infrared, which increases when the vegetation activity becomes more active. The red band (Band 4) and NIR band (Band 8) are used in combination defined as follows [13].

$$NDVI = \frac{Band\ 8 - Band\ 4}{Band\ 8 + Band\ 4} \quad (2)$$

NDWI is an index that is widely used for vegetation analysis by using the difference of spectral characteristics according to moisture content in vegetation [16]. The difference between NIR and SWIR, and the difference between green and SWIR, are the widely used methods [37]. In this study, two types of NDWIs were generated using the difference between green (Band 3) and SWIR (Band 11, Band 12) as follows [39].

$$NDWI_1 = \frac{Band\ 3 - Band\ 11}{Band\ 3 + Band\ 11} \quad (3)$$

$$NDWI_2 = \frac{Band\ 3 - Band\ 12}{Band\ 3 + Band\ 12} \quad (4)$$

NDre is an index using vegetation red edge band, indicating that the higher the NDre value, the greater the activity of vegetation. In this study, two types of NDre were created using three red edge bands (Bands 5–7) provided by Sentinel-2 [40,41].

$$NDre_1 = \frac{Band\ 6 - Band\ 5}{Band\ 6 + Band\ 5} \quad (5)$$

$$NDre_2 = \frac{Band\ 7 - Band\ 5}{Band\ 7 + Band\ 5} \quad (6)$$

In addition, texture data were used to visually consider the difference in the forest texture and the reflectivity of forest communities according to the dominant species. In the RGB image, the texture of the image is determined by the distribution of shadows. In the case of the artificial forest of the single-layer structure having the same number of species and ages, the texture is smooth due to the constant height between the trees. Multi-layered natural forests of varying ages and species are roughly textured [18]. It is also considered that the arrangement of canopies is uniform in single-layer forests and uneven in multi-layer forests [18,22]. To take this into account, the PCA, which is a representative dimensional reduction feature extraction technique used in multiband image processing, was used [42]. An image that has undergone the PCA technique has the advantage of showing surface characteristics and spectral information that were difficult to read from the original image [43].

The calculation of the PCA texture maps is conducted by three steps: (1) generation of base map by applying a 5×5 median filter to the produced PCA image with the moving window technique, (2) subtracting a texture image from the PCA image and applying the root mean square deviation equation, and (3) applying a 3×3 median filter to the texture image to reduce unwanted noise information. The final PCA texture map was produced by converting the calculated image value into a DB unit [37,44] as follows.

$$Texture_{db}(i, j) = -20 \cdot \log_{10}(Texture(i, j)) \quad (7)$$

3.1.2. Canopy Height Maps from DSM and DTM

Finally, DTM and DSM data were collected for the forest height measurement. The DTM used in this study is a 5 m DEM produced by the National Geographic Information Institute (NGII) (Figure 5a). For DSM, 12 m resolution WorldDEM data were obtained which is created by using TerraSAR-X

X-band radar interferometry (Figure 5b) from German Aerospace Center (Deutsches Zentrum für Luft- und Raumfahrt e.V., DLR). Both data were resampled into 10 m based on the GSD (Ground Sample Distance) of the Sentinel-2 image, and the forest height map was generated by subtracting DTM which means the terrain height of ground and DSM data which includes the height of ground objects such as canopies and buildings. The canopy height map was created. In addition, DSM data were used to correct the terrain of Sentinel-2 images.

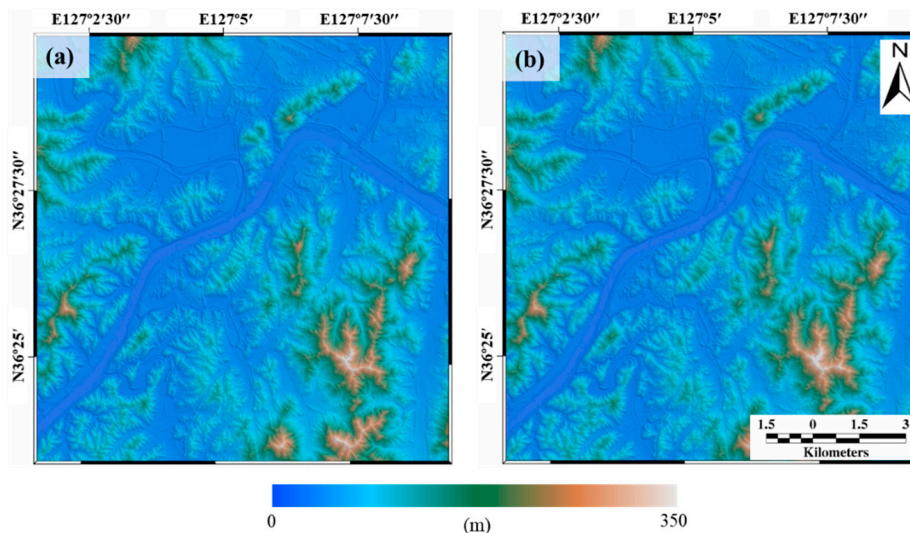


Figure 5. (a) Digital Terrain model (10 m) from national geographic information institute (NGII). (b) WorldDEM (12 m).

In addition, the canopy height maps were created in consideration of the fact that the forest vertical structure is closely related to the canopy height. The canopy height map is effective for measuring tree height over large areas which could be calculated from the difference between DSM and DTM [23]. In this study, 5 m resolution DTM (NGII DEM) generated based on 1:5000 digital topographic maps (NGII, Suwon, South Korea) and the 12 m resolution DSM (WorldDEM) generated using the TerraSAR-X SAR interferometry (InSAR) were resampled to 10 m as Sentinel-2 image and used to extract the canopy height from German Aerospace Center (Deutsches Zentrum für Luft- und Raumfahrt e.V., DLR). Average canopy height and standard deviation canopy height maps were generated by calculating the mean and standard deviation in a window with the kernel of 5×5 .

DTM data could be less accurate in slope areas, and DSM could be underestimated as radar signals penetrate through forest areas. Thus, the average canopy height map estimated from InSAR-based DSMs may appear somewhat lower than the actual canopy. The standard deviation canopy height map shows higher values in areas with large differences in canopy heights and smaller values in smooth areas. As such, the height of the forest that shows the distribution characteristics of the forest existing in the image could be calculated by subtracting the DTM in the DSM.

3.2. Application of Artificial Neural Network

The machine learning model of ANN with MultiLayer Perceptron (MLP) algorithm was used for learning in this study. The MLP algorithm adds hidden layers to compensate for the limitation of the linear classification of the conventional perceptron [45]. The MLP algorithm consists of three groups of layers: input layer, hidden layer, and output layer. The MLP algorithm adjusts the connection strength between layers and processes it repeatedly to perform prediction and estimation by using the error back propagation learning technique for learning. In the error back algorithm, an input signal is transmitted to a hidden layer through a feedforward network and generates the final output. The weight is corrected by propagating the error in the direction of reducing the error by comparing the

output with the true value. An activation function is used to adjust the strength of the connection. In this study, logistic function, the commonly used unipolar sigmoid function, is used as follows.

$$\sigma(z) = \frac{1}{1 + \exp(-z)} \quad (8)$$

This function adjusts the result to a value between 0 and 1, which represents the result with a probability of 0 to 1 [46].

The input layers of NDVI, two types of NDWI, two types of NDre, PCA Texture, average canopy height, and standard deviation canopy height map produced from the above process are assumed to be correlated with forest vertical structure. To estimate the forest vertical structure, Waikato Environment for Knowledge Analysis (WEKA), a widely used data mining tool, was used in this study [47]. Training (70%) and test (30%) data were randomly set for each layer. Training (including validation) was processed with 70% (1,608,912 pixels including 297,365, 186,573, 1,124,975 for single-, double- and triple-layers, respectively) and test was performed with rest of data. The training and validation process of ANN algorithms were performed by using 10-fold cross validation technique; it is a method of repeating the training and validation by dividing the training and validation set into 10 and finding the optimal condition by the average of the errors recorded in each fold attempt to tune the optimal hyperparameters. For this purpose, the training/validation dataset was divided into 10 groups with nine groups of training data and one group of validation data; each group was used once for validation and nine times for training. Finally, forest vertical structure classification was conducted using the preprocessed data above as an input layer to the ANN and test accuracy was calculated by using test dataset.

4. Results

In this study, MLP-ANN method is applied to map forest vertical structure in Gongju-si, which is located near the center of South Korea. Fourteen input neurons generated from Sentinel-2 optical satellite images, existing DTM and DSM data were used as input layers for the MLP-ANN approach.

4.1. Results Maps from Preprocessing

A total of 12 neurons were prepared by Sentinel-2 optical satellite images of spring and fall season, 6 input data were generated each: NDVI, NDWI1, NDWI2, NDre1, NDre2, and PCA texture. Figures 6–8 show the NDVI, NDWI, and NDre maps of Sentinel-2 represented by using ArcMap 10.4 (ESRI, Redlands, CA, USA). Preprocessed Sentinel-2 images with a Statistical-empirical model shows very little topographic effect even in mountain slope area (see Figures 6–8).

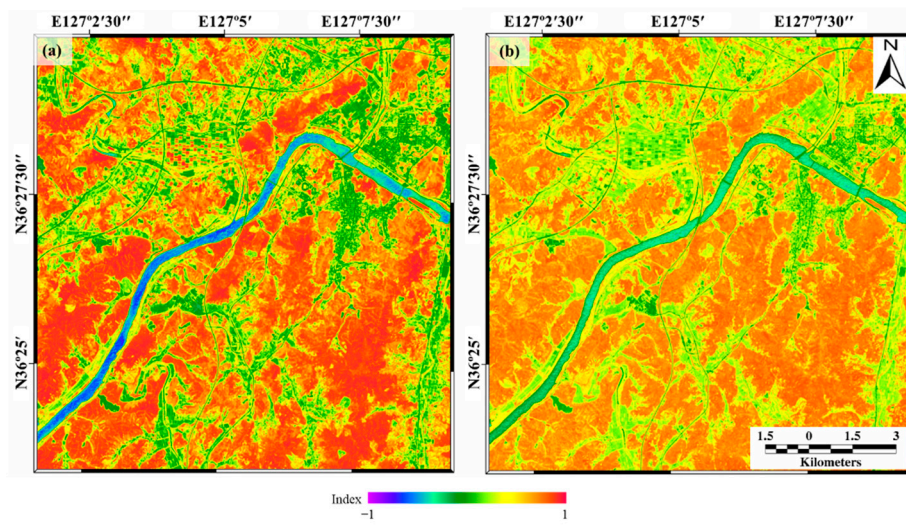


Figure 6. Input neurons of NDVI created from Sentinel-2 image: (a) spring and (b) fall season.

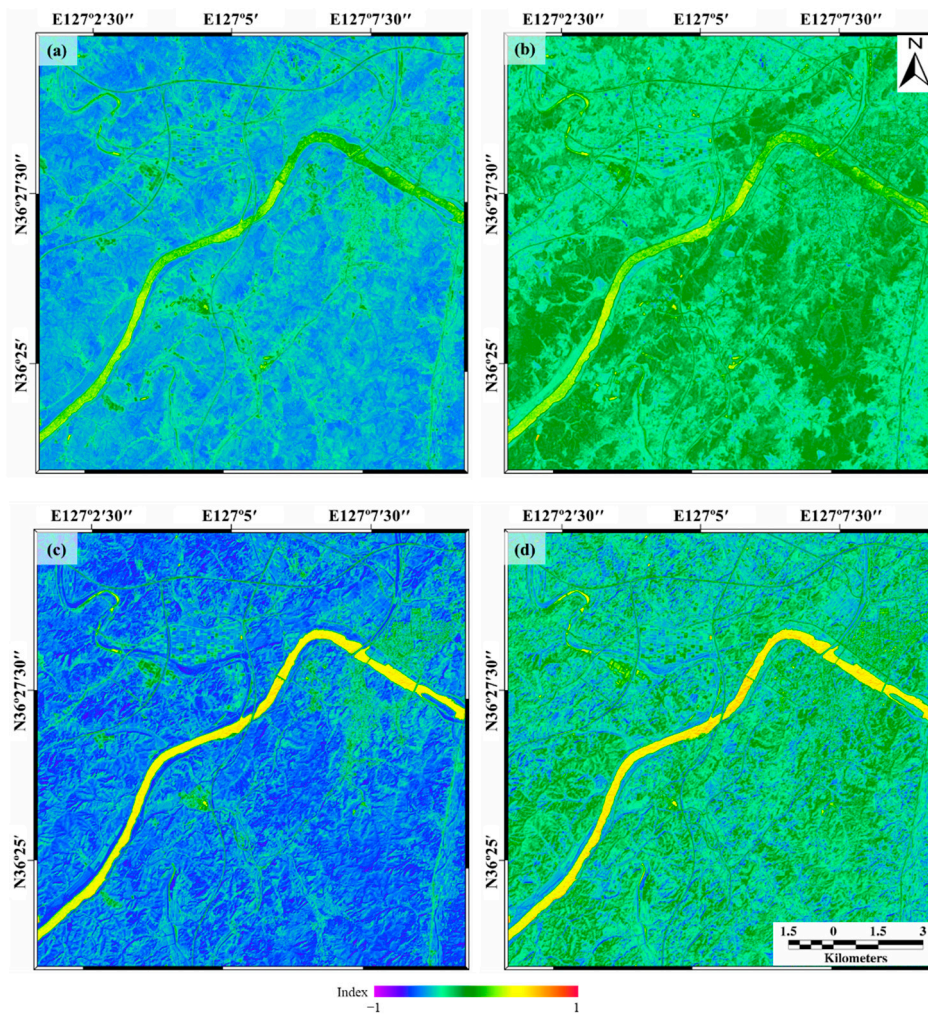


Figure 7. Input neurons of NDWI1 and NDWI2 created from Sentinel-2 image: (a) NDWI1 in spring and (b) fall season, (c) NDWI2 in spring and (d) fall season.

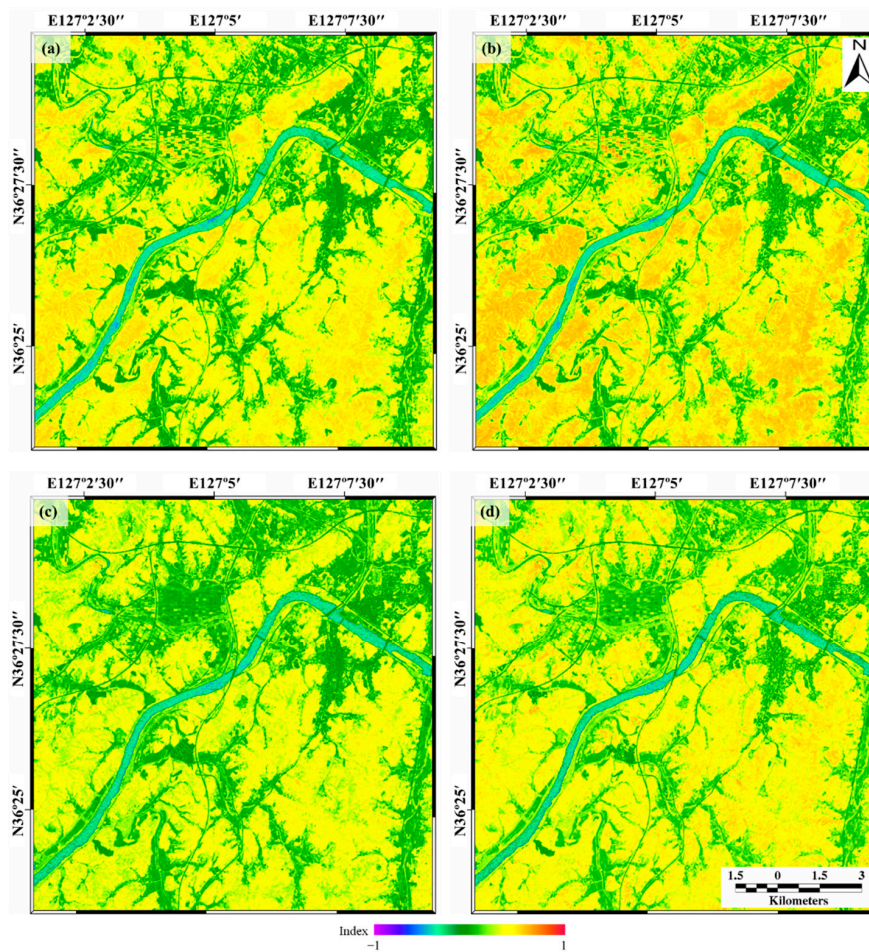


Figure 8. Input neurons of NDre1 and NDre2 created from Sentinel-2 image: (a) NDre1 images in spring and (b) fall season, (c) NDre2 images in spring and (d) fall season.

In addition, PCA texture maps were generated using Equations (4) and (5) from seasonal Sentinel-2 optic satellite images, respectively. The smoother the surface, the higher the texture values as shown in Figure 9a,b.

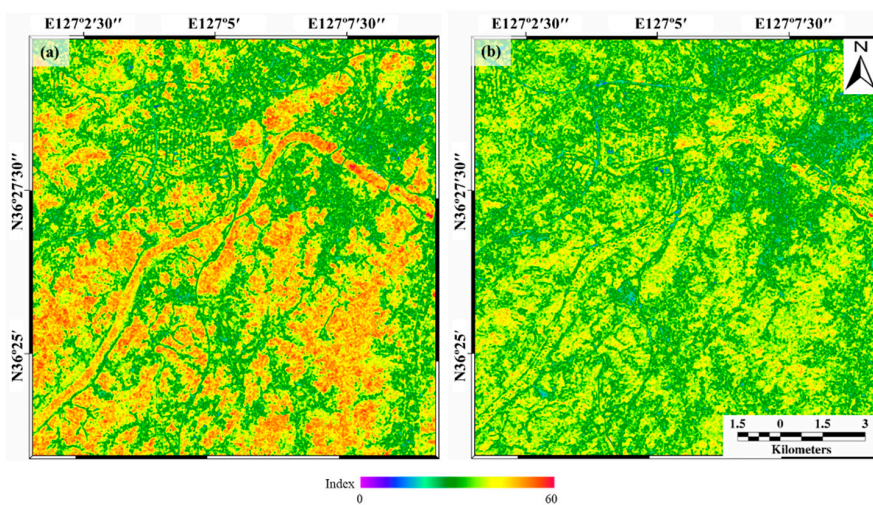


Figure 9. Input neurons of PCA texture created from Sentinel-2 image: (a) spring and (b) fall season.

The other two input neurons were generated by differentiating the DTM obtained from NGII and the DSM obtained from WorldDEM as described above. From the canopy height map obtained from this process, two data were generated by a moving window technique with the kernel of 5×5 . The first kind of canopy height map is an average canopy height map that could be used to estimate the average height of the canopies in the forest as shown in Figure 10a. Most average values range from 7 m to 15 m, with average values up to 25 m in some regions. Another canopy height map is a standard deviation canopy height map that reflects the varying heights of adjacent trees (Figure 10b). The varying vertical structure of forest means that there is a difference in the canopy height, so the standard deviation of the height data was obtained to recognize the difference in height of adjacent trees. In other words, the higher the standard deviation in forest region, the larger the difference in the tree height of the region, which leads to complicated vertical structure of the forest.

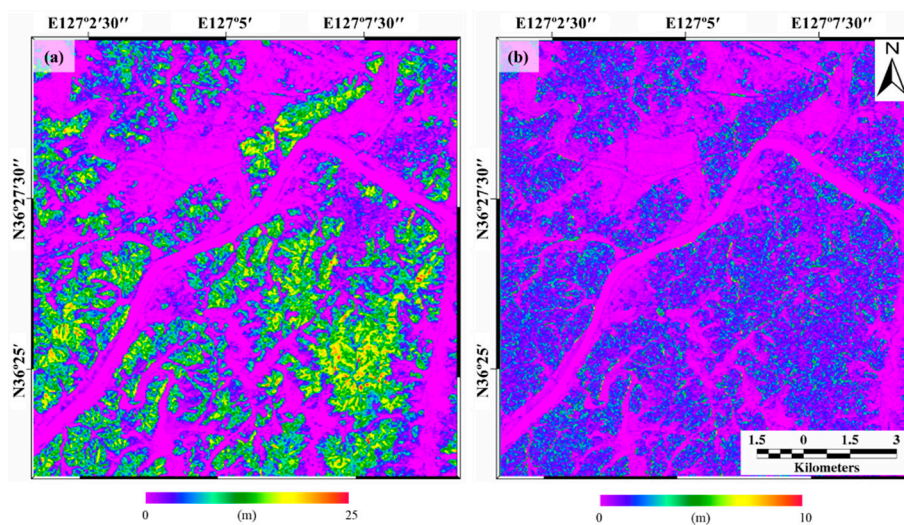


Figure 10. Canopy height maps estimated from DSM and DTM: (a) average canopy height map and (b) standard deviation canopy height map.

4.2. Results from Artificial Neural Network

As a result from ANN approaches, probability maps for each vertical structure were obtained as shown in Figure 11: (a) single-layer structure, (b) double-layer structure, and (c) triple-layer structure. As aforementioned, the single-, double-, and triple-layer structures in this study are defined by how many layers it contains among the canopy layer, the understory layer, and the shrub layer. In the probability maps, most pixels of a single-layer structure probability map have relatively low values of less than 10%. Some pixels of the double layer probability maps have low values of less than 20%, whereas others have values between 40% and 60%. In the case of a triple-layer structure probability map, some pixels have a probability value higher than 70%, and the outer pixels of the forest appear to have a probability value lower than 20%.

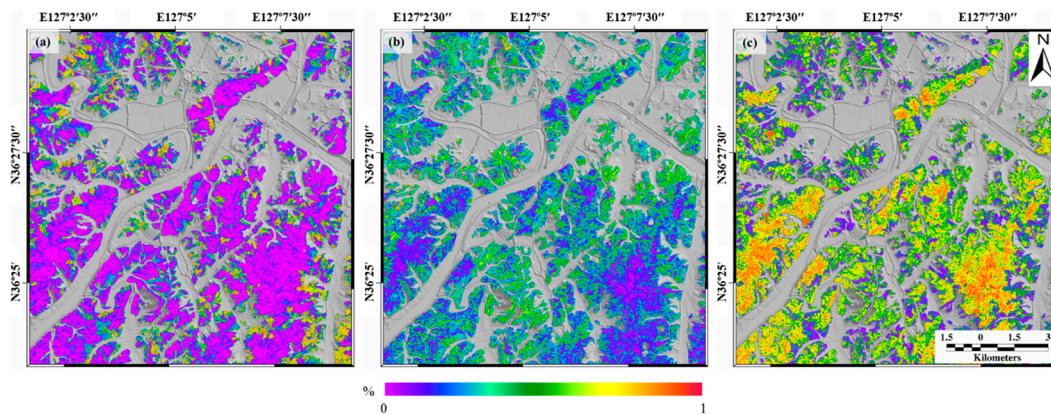


Figure 11. Probability maps of forest vertical structure using ANN approach: (a) single-layer, (b) double-layer, and (c) triple-layer.

A high percentage of low values in the single- and double-layer structure probability maps indicates that there is a relatively small percentage of single- and double-layer forests in the study area. In a triple-layer structure probability map, probability values greater than 70% indicate a high probability for a triple-layer structure forest, whereas probability values lower than 20% indicate little or no triple-layer structure, which means that the triple structure could be clearly distinguished. In addition, the probability of a triple-layer forest occupies most of the study area since the probability density function of triple-layer structure is closer to the Gaussian distribution than the single- and double-layer structure forests.

The final classification map was created using the maximum operation that considers the highest value in the same pixel of each layer’s probability map (Figure 12). The probability of single- and double-layer structure maps was relatively low, so that the percentage of single- (20%) and double-layer (15%) structure area was low; the triple-layer structure forests dominate with 65% in the study area as represented in the classification map. As the study area is mostly composed of multi-layered natural forests, the classification results are considered to be in line with expectations.

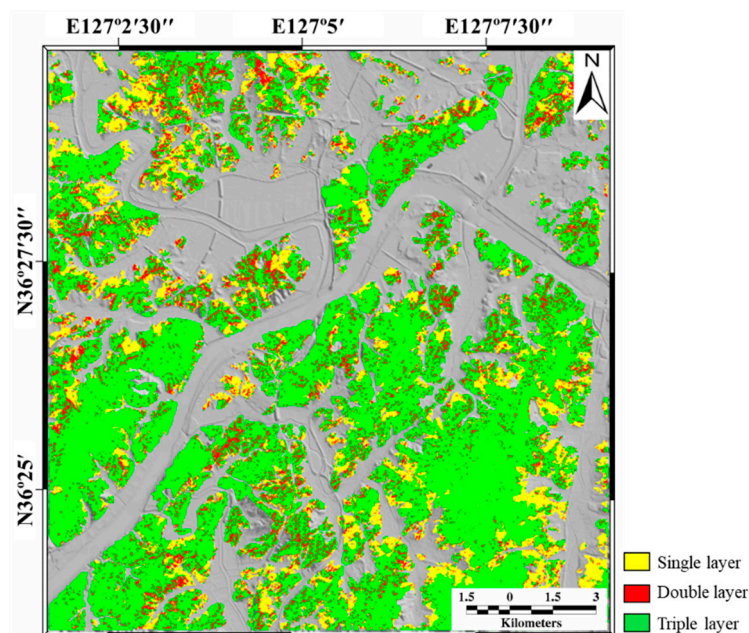


Figure 12. Forest vertical structure map classified from forest vertical probability maps using the maximum operation.

The classification map was evaluated for accuracy, as shown in Table 3, through the error matrix based on the forest vertical structure data based on the field survey of Figure 2a. The total number of test data pixels excluding non-forest areas is 689,534. The overall test accuracy for the total pixels estimated from the error matrix was ~65.06%, which was not very high. The application of ANN approach with full-waveform Lidar data could expect higher accuracy. However, full-waveform Lidar data is difficult to build for large areas at a single time, and is difficult to use for most areas because of the high cost. Optical satellite images and topographic data including DSM and DTM are available for most parts of the world, which could be used for cost- and time-efficient production of forest vertical maps. As a result, it is possible to observe the forest vertical structure over a large area using optical images and topographic data with ~65% accuracy.

Table 3. Validation of forest vertical structure classified by using the ANN (unit: pixel).

Reference \ ANN	Single Layer	Double Layer	Triple Layer	Total	User Accuracy (%)
Single Layer	71,952	9,904	59,110	140,966	51.04%
Double Layer	15,421	20,170	66,624	102,215	19.73%
Triple Layer	40,069	49,886	356,398	446,353	79.85%
Total	127,442	79,960	482,132	689,534	
Producer accuracy (%)	56.46%	25.23%	73.92%		
Overall accuracy (%)			65.06%		

The user and producer accuracy in single-layer structure was approximately 51.04% and 56.46%, respectively, with more than half the accuracy. Double-layer forests have 19.73% and 25.23% user and producer accuracy, respectively, which could be represented to have been identified with very low probability. This is due to the fact that there are very few data in the double-layer forest for training and testing the MLP-ANN model, and ~62.3% of the double-layer structure has been misclassified as a triple-layer structure due to the similar canopy characteristics of the double-layer and triple-layer forests. Therefore, it could be mentioned that 62.3% of double-layer forests are very similar to the pattern of triple-layer forests. This result in this study means that a double-layer structured area cannot be completely separated from a triple-layer structure forest. The user and producer accuracy in triple-layer structure forest is about 79.85% and 73.92%, respectively. Triple-layer structure accuracy was higher than the accuracy of single- and double-structure. It can be interpreted that this is due to the well-trained MLP ANN model parameters in the triple-layer structure. Nevertheless, about 12.3% and 13.8% of the triple-layer structure were misclassified as single- and as double-layer forests, respectively.

To analyze the cause of the misclassification, the forest map and the original Sentinel-2 RGB image were compared and analyzed by visual interpretation. As a result, it was confirmed that forest trees were artificially removed or newly formed in the single-, double-, and triple-layer structure, as shown in Figure 13. This type of misclassification is occurred due to the time difference between the acquisition time of satellite images and the field survey, which could lead to the learning and output of ANN algorithm.

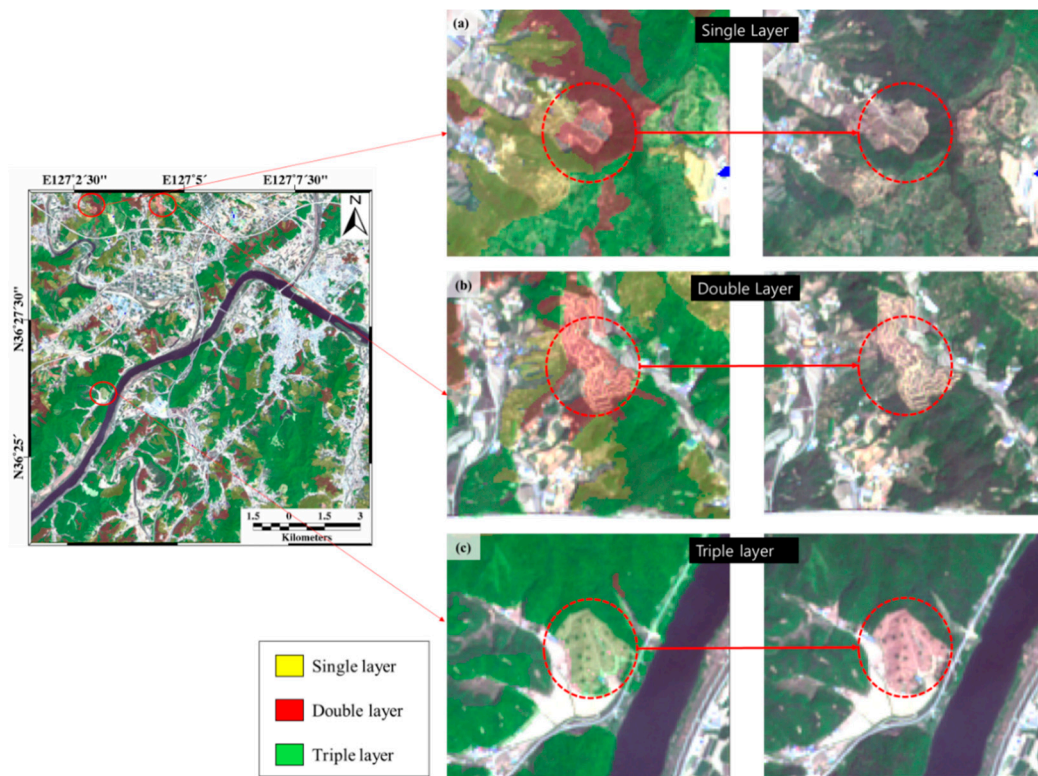


Figure 13. The forest vertical classification map with the original Sentinel-2 RGB image. (a) single-layer, (b) double-layer and (c) triple-layer structure forest.

5. Conclusions

The purpose of this study is to analyze forest vertical structure in Gongju-si to enhance the function of forest related to water resource management. MLP-ANN model machine learning technology was applied to Sentinel-2 optical satellite images and previously constructed DTM and DSM data. Machine learning techniques can be applied based on large amounts of remote sensing data to produce information about continuous internal structures in areas with high uncertainty. Therefore, input data NDVI, NDWI1, NDWI2, NDre1, NDre2, and PCA texture maps were generated from Sentinel-2 optical satellite images. In addition, an average canopy height map and a standard deviation canopy height map were generated from DTM and DSM. The classification result from ANN shows that the triple-layer forest with the highest water reserves has shown a relatively accurate 73.92% classification in producer accuracy.

Understanding the vertical structure of forests is essential for estimating forest water storage capacity for integrated water management. The results of this study show that the satellite image data, including optical satellite images and DEM data, could be used for more accurate estimation of the forest water storage by constructing data on forest vertical structures. Therefore, more accurate water storage on forest could be estimated using the vertical structure constructed using satellite images along with the forest type data provided from the forest map.

The diversity of vertical structures with the various age of forests could improve the soil penetrating structure of rainwater and increase the amount of water the forest can store. However, estimation of the forest structure in a large area is difficult due to its difficult accessibility and various forms; it is necessary to use periodic satellite images for estimating vertical structures in national-scale forests which could support forest management for water resource management. Also, the combination of remote sensing, which is essential for exploring large areas, and machine learning, which is effective for classifying and analyzing large amounts of data, could be very useful as in this study. Especially, as there is a limit in obtaining information on the internal structure of forests, it is possible to estimate the

vertical structure of the forest through the methodology applied in this study using remote sensing satellite imagery and machine learning technology. It is also expected to reduce research costs, such as time and budget for field surveys.

In this study, the degradation of the learning and classification results was derived using the data with the difference between the acquisition time of the image and the investigation time of the reference data. In the future study, images of similar time should be collected to reflect the difference in survey time and improved results could be expected by obtaining reference data from multiple regions with different forest types. Additionally, various deep learning technologies which are being developed recently could reflect the detailed characteristics of the images. Based on the results of this study, the forest vertical structure data through remote sensing and machine learning could be used to estimate the forest water storage and establish forest administration measures for integrated water management.

Author Contributions: Conceptualization, H.-S.J.; methodology, Y.-S.L., S.L., and H.-S.J.; software, Y.-S.L. and S.L.; validation, Y.-S.L. and S.L.; formal analysis, Y.-S.L., S.L., and H.-S.J.; investigation, Y.-S.L., S.L., and H.-S.J.; writing—original draft preparation, Y.-S.L. and S.L.; writing—review and editing, S.L. and H.-S.J.; supervision, H.-S.J. All authors have read and agreed to the published version of the manuscript.

Funding: This work was supported by the National Research Foundation of Korea funded by the Korea government under Grant NRF-2018M1A3A3A02066008, and it was also conducted at Korea Environment Institute (KEI) with support from the Basic Science Research Program funded by the National Research Foundation of Korea (NRF) via Grant NRF-2018R1D1A1B07041203.

Conflicts of Interest: The authors declare no conflict of interest.

References

1. Luo, P.; Zhou, M.; Deng, H.; Lyu, J.; Cao, W.; Takara, K.; Nover, D.; Schladow, S.G. Impact of forest maintenance on water shortages: Hydrologic modeling and effects of climate change. *Sci. Total Environ.* **2018**, *615*, 1355–1363. [[CrossRef](#)] [[PubMed](#)]
2. Keleş, S. An assessment of hydrological functions of forest ecosystems to support sustainable forest management. *J. Sustain. For.* **2019**, *38*, 305–326. [[CrossRef](#)]
3. Terêncio, D.; Fernandes, L.S.; Cortes, R.; Moura, J.; Pacheco, F. Rainwater harvesting in catchments for agro-forestry uses: A study focused on the balance between sustainability values and storage capacity. *Sci. Total Environ.* **2018**, *613*, 1079–1092. [[CrossRef](#)] [[PubMed](#)]
4. Creed, I.F.; Jones, J.J.; Archer Van Garderen, E.; Claassen, M.; Ellison, D.; McNulty, S.G.; Van Noordwijk, M.; Vira, B.; Wei, X.; Bishop, K. Managing Forests for Both Downstream and Downwind Water. *Front. For. Glob. Chang.* **2019**, *2*, 64. [[CrossRef](#)]
5. Sun, J.; Yu, X.; Wang, H.; Jia, G.; Zhao, Y.; Tu, Z.; Deng, W.; Jia, J.; Chen, J. Effects of forest structure on hydrological processes in China. *J. Hydrol.* **2018**, *561*, 187–199. [[CrossRef](#)]
6. Murai, T.; Andrews, J.W. Interactions of dietary α -tocopherol, oxidized menhaden oil and ethoxyquin on channel catfish (*Ictalurus punctatus*). *J. Nutr.* **1974**, *104*, 1416–1431. [[CrossRef](#)]
7. Yu, Z.; Liu, S.; Wang, J.; Wei, X.; Schuler, J.; Sun, P.; Harper, R.; Zegre, N. Natural forests exhibit higher carbon sequestration and lower water consumption than planted forests in China. *Glob. Chang. Biol.* **2019**, *25*, 68–77. [[CrossRef](#)]
8. Clark, M.L.; Buck-Diaz, J.; Evens, J. Mapping of forest alliances with simulated multi-seasonal hyperspectral satellite imagery. *Remote Sens. Environ.* **2018**, *210*, 490–507. [[CrossRef](#)]
9. Morin, D.; Planells, M.; Guyon, D.; Villard, L.; Mermoz, S.; Bouvet, A.; Thevenon, H.; Dejoux, J.-F.; Le Toan, T.; Dedieu, G. Estimation and Mapping of Forest Structure Parameters from Open Access Satellite Images: Development of a Generic Method with a Study Case on Coniferous Plantation. *Remote Sens.* **2019**, *11*, 1275. [[CrossRef](#)]
10. Taureau, F.; Robin, M.; Proisy, C.; Fromard, F.; Imbert, D.; Debaine, F. Mapping the mangrove forest canopy using spectral unmixing of very high spatial resolution satellite images. *Remote Sens.* **2019**, *11*, 367. [[CrossRef](#)]
11. Liu, J.; Zhang, Z.; Zhang, M. Impacts of forest structure on precipitation interception and run-off generation in a semiarid region in northern China. *Hydrol. Process.* **2018**, *32*, 2362–2376. [[CrossRef](#)]

12. Cho, H.; Lee, K.-S. Comparison between hyperspectral and multispectral images for the classification of coniferous species. *Korean J. Remote Sens.* **2014**, *30*, 25–36. [[CrossRef](#)]
13. Krieglner, F.; Malila, W.; Nalepka, R.; Richardson, W. Preprocessing Transformations and Their Effects on Multispectral Recognition. In Proceedings of the Sixth International Symposium on Remote Sensing of Environment, Ann Arbor, MI, USA, 13–16 October 1969; p. 97.
14. Gao, B.-C. NDWI—A normalized difference water index for remote sensing of vegetation liquid water from space. *Remote Sens. Environ.* **1996**, *58*, 257–266. [[CrossRef](#)]
15. Delegido, J.; Verrelst, J.; Alonso, L.; Moreno, J. Evaluation of sentinel-2 red-edge bands for empirical estimation of green LAI and chlorophyll content. *Sensors* **2011**, *11*, 7063–7081. [[CrossRef](#)] [[PubMed](#)]
16. Lee, B.; Kim, E.S.; Lee, J.-S.; Jung, J.; Lim, J.H. Detecting Phenology Using MODIS Vegetation Indices and Forest Type Map in South Korea. *Korean J. Remote Sens.* **2018**, *34*, 267–282.
17. Herrmann, I.; Pimstein, A.; Karnieli, A.; Cohen, Y.; Alchanatis, V.; Bonfil, D. LAI assessment of wheat and potato crops by VEN μ S and Sentinel-2 bands. *Remote Sens. Environ.* **2011**, *115*, 2141–2151. [[CrossRef](#)]
18. Hay, G.; Niemann, K.; McLean, G. An object-specific image-texture analysis of H-resolution forest imagery. *Remote Sens. Environ.* **1996**, *55*, 108–122. [[CrossRef](#)]
19. Morsdorf, F.; Mårell, A.; Koetz, B.; Cassagne, N.; Pimont, F.; Rigolot, E.; Allgöwer, B. Discrimination of vegetation strata in a multi-layered Mediterranean forest ecosystem using height and intensity information derived from airborne laser scanning. *Remote Sens. Environ.* **2010**, *114*, 1403–1415. [[CrossRef](#)]
20. Mund, J.-P.; Wilke, R.; Körner, M.; Schultz, A. Detecting multi-layered forest stands using high density airborne LiDAR data. *J. Geogr. Inf. Sci.* **2015**, *1*, 178–188. [[CrossRef](#)]
21. Zimble, D.A.; Evans, D.L.; Carlson, G.C.; Parker, R.C.; Grado, S.C.; Gerard, P.D. Characterizing vertical forest structure using small-footprint airborne LiDAR. *Remote Sens. Environ.* **2003**, *87*, 171–182. [[CrossRef](#)]
22. Kwon, S.-K.; Jung, H.-S.; Baek, W.-K.; Kim, D. Classification of forest vertical structure in south Korea from aerial orthophoto and lidar data using an artificial neural network. *Appl. Sci.* **2017**, *7*, 1046. [[CrossRef](#)]
23. Sadeghi, Y.; St-Onge, B.; Leblon, B.; Simard, M. Canopy height model (CHM) derived from a TanDEM-X InSAR DSM and an airborne lidar DTM in boreal forest. *IEEE J. Sel. Top. Appl. Earth Obs. Remote Sens.* **2016**, *9*, 381–397. [[CrossRef](#)]
24. Fu, H.; Wang, C.; Zhu, J.; Xie, Q.; Zhang, B. Estimation of pine forest height and underlying DEM using multi-baseline P-band PolInSAR data. *Remote Sens.* **2016**, *8*, 820. [[CrossRef](#)]
25. Sun, G.; Ranson, K.; Kimes, D.; Blair, J.; Kovacs, K. Forest vertical structure from GLAS: An evaluation using LVIS and SRTM data. *Remote Sens. Environ.* **2008**, *112*, 107–117. [[CrossRef](#)]
26. Lary, D.J.; Alavi, A.H.; Gandomi, A.H.; Walker, A.L. Machine learning in geosciences and remote sensing. *Geosci. Front.* **2016**, *7*, 3–10. [[CrossRef](#)]
27. Li, W.; Cao, S.; Campos-Vargas, C.; Sanchez-Azofeifa, A. Identifying tropical dry forests extent and succession via the use of machine learning techniques. *Int. J. Appl. Earth Obs. Geoinf.* **2017**, *63*, 196–205. [[CrossRef](#)]
28. Stojanova, D.; Panov, P.; Gjorgjioski, V.; Kobler, A.; Džeroski, S. Estimating vegetation height and canopy cover from remotely sensed data with machine learning. *Ecol. Inform.* **2010**, *5*, 256–266. [[CrossRef](#)]
29. Zhao, K.; Popescu, S.; Meng, X.; Pang, Y.; Agca, M. Characterizing forest canopy structure with lidar composite metrics and machine learning. *Remote Sens. Environ.* **2011**, *115*, 1978–1996. [[CrossRef](#)]
30. Bazi, Y.; Melgani, F. Toward an optimal SVM classification system for hyperspectral remote sensing images. *IEEE Trans. Geosci. Remote Sens.* **2006**, *44*, 3374–3385. [[CrossRef](#)]
31. Yuan, H.; Yang, G.; Li, C.; Wang, Y.; Liu, J.; Yu, H.; Feng, H.; Xu, B.; Zhao, X.; Yang, X. Retrieving soybean leaf area index from unmanned aerial vehicle hyperspectral remote sensing: Analysis of RF, ANN, and SVM regression models. *Remote Sens.* **2017**, *9*, 309. [[CrossRef](#)]
32. Belgiu, M.; Drăguț, L. Random forest in remote sensing: A review of applications and future directions. *ISPRS J. Photogramm. Remote Sens.* **2016**, *114*, 24–31. [[CrossRef](#)]
33. Ashby, J.; Moreno-Madrinán, M.J.; Yiannoutsos, C.T.; Stanforth, A. Niche modeling of dengue fever using remotely sensed environmental factors and boosted regression trees. *Remote Sens.* **2017**, *9*, 328. [[CrossRef](#)]
34. Ghatkar, J.G.; Singh, R.K.; Shanmugam, P. Classification of algal bloom species from remote sensing data using an extreme gradient boosted decision tree model. *Int. J. Remote Sens.* **2019**, *40*, 9412–9438. [[CrossRef](#)]
35. National Institute of Ecology. *The 3rd National Natural Environment Survey*, 3rd ed.; National Natural Environment Survey: Seoul, Korea, 2009.

36. Drusch, M.; Del Bello, U.; Carlier, S.; Colin, O.; Fernandez, V.; Gascon, F.; Hoersch, B.; Isola, C.; Laberinti, P.; Martimort, P. Sentinel-2: ESA's optical high-resolution mission for GMES operational services. *Remote Sens. Environ.* **2012**, *120*, 25–36. [[CrossRef](#)]
37. Kwon, S.-K. *Classification of Natural Forest/Artificial Forest from Sentinel-2 Images Using Artificial Neural Network*; University of Seoul: Seoul, Korea, 2018.
38. Teillet, P.; Guindon, B.; Goodenough, D. On the slope-aspect correction of multispectral scanner data. *Can. J. Remote Sens.* **1982**, *8*, 84–106. [[CrossRef](#)]
39. McFeeters, S.K. The use of the Normalized Difference Water Index (NDWI) in the delineation of open water features. *Int. J. Remote Sens.* **1996**, *17*, 1425–1432. [[CrossRef](#)]
40. Barnes, E.; Clarke, T.; Richards, S.; Colaizzi, P.; Haberland, J.; Kostrzewski, M.; Waller, P.; Choi, C.; Riley, E.; Thompson, T. Coincident Detection of Crop Water Stress, Nitrogen Status and Canopy Density Using Ground Based Multispectral Data. In Proceedings of the Fifth International Conference on Precision Agriculture, Bloomington, MN, USA, 16–19 July 2000.
41. Gitelson, A.; Merzlyak, M.N. Spectral reflectance changes associated with autumn senescence of *Aesculus hippocastanum* L. and *Acer platanoides* L. leaves. Spectral features and relation to chlorophyll estimation. *J. Plant Physiol.* **1994**, *143*, 286–292. [[CrossRef](#)]
42. Yoon, S.; Lee, S.; Park, K.; Jang, S.; Rhee, J. Development of a Storage Level and Capacity Monitoring and Forecasting Techniques in Yongdam Dam Basin Using High Resolution Satellite Image. *J. Korean J. Remote Sens.* **2018**, *34*, 1041–1053.
43. Yang, C.; Lu, L.; Lin, H.; Guan, R.; Shi, X.; Liang, Y. A fuzzy-statistics-based principal component analysis (FS-PCA) method for multispectral image enhancement and display. *IEEE Trans. Geosci. Remote Sens.* **2008**, *46*, 3937–3947. [[CrossRef](#)]
44. Lillesand, T.M.; Kiefer, R.W.; Chipman, J. *Remote Sensing and Image Interpretation*; John Wiley & Sons: New York, NY, USA, 2000; p. 724.
45. Lee, Y.-S.; Park, S.-H.; Jung, H.-S.; Baek, W.-K. Classification of Natural and Artificial Forests from KOMPSAT-3/3A/5 Images Using Artificial Neural Network. *Korean J. Remote Sens.* **2018**, *34*, 1399–1414.
46. Hwang, J.-I.; Jung, H.-S. Automatic ship detection using the artificial neural network and support vector machine from X-band SAR satellite images. *Remote Sens.* **2018**, *10*, 1799. [[CrossRef](#)]
47. Witten, I.H.; Frank, E.; Hall, M.A.; Pal, C. *Data Mining: Practical Machine Learning Tools and Techniques*; Morgan Kaufmann: Burlington, MA, USA, 2016.



© 2020 by the authors. Licensee MDPI, Basel, Switzerland. This article is an open access article distributed under the terms and conditions of the Creative Commons Attribution (CC BY) license (<http://creativecommons.org/licenses/by/4.0/>).